Untangle charge-order dependent bulk states from surface effects in a topological kagome metal ScV_6Sn_6

Zi-Jia Cheng,[1,*] Sen Shao,[2] Byunghoon Kim,[1] Tyler A. Cochran,[1] Xian P. Yang,[1] Changjiang Yi,[3] Yu-Xiao Jiang,[1] Junyi Zhang,[4] Md Shafayat Hossain,[1] Subhajit Roychowdhury,[3] Turgut Yilmaz,[5] Elio Vescovo,[5] Alexei Fedorov,[6] Shekhar Chandra,[3] Claudia Felser,[3] Guoqing Chang,[2,†] and M.Zahid Hasan[1,‡]

[1] *Laboratory for Topological Quantum Matter and Advanced Spectroscopy (B7), Department of Physics, Princeton University, Princeton, New Jersey 08544, USA*
[2] *Division of Physics and Applied Physics, School of Physical and Mathematical Sciences, Nanyang Technological University, 21 Nanyang Link, 637371, Singapore*
[3] *Max Planck Institute for Chemical Physics of Solids, Nöthnitzer Straße 40, Dresden, 01187, Germany*
[4] *Institute for Quantum Matter and Department of Physics and Astronomy, Johns Hopkins University, Baltimore, Maryland 21218, USA*
[5] *National Synchrotron Light Source II, Brookhaven National Laboratory, Upton, New York 11973, USA*
[6] *Advanced Light Source, Lawrence Berkeley National Laboratory, Berkeley, CA 94720, USA*

Kagome metals with charge density wave (CDW) order exhibit a broad spectrum of intriguing quantum phenomena. The recent discovery of the novel kagome CDW compound ScV_6Sn_6 has spurred significant interest. However, understanding the interplay between CDW and the bulk electronic structure has been obscured by a profusion of surface states and terminations in this quantum material. Here, we employ photoemission spectroscopy and potassium dosing to elucidate the complete bulk band structure of ScV_6Sn_6 , revealing multiple van Hove singularities near the Fermi level. We surprisingly discover a robust spin-polarized topological Dirac surface resonance state at the M point within the two-fold van Hove singularities. Assisted by the first-principle calculations, the temperature dependence of the k_z- resolved ARPES spectrum provides unequivocal evidence for the proposed $\sqrt{3}\times\sqrt{3}\times3$ charge order over other candidates. Our work not only enhances the understanding of the CDW-dependent bulk and surface states in ScV_6Sn_6 but also establishes an essential foundation for potential manipulation of the CDW order in kagome materials.

I. INTRODUCTION

Charge density wave (CDW), a collective quantum phenomenon wherein the electron density undergoes a periodic modulation, have long been extensively investigated in condensed matter physics[1–4]. Arising from electron-lattice or electron-electron interactions, CDWs can compete with or coexist alongside other unconventional quantum states and offer a window into the complex behavior of correlated electrons[5–7]. The emergence of CDWs in kagome metals has infused a fresh perspective into this field[8, 9]. Kagome metals, characterized by the distinctive frustrated lattice, furnish a valuable platform for exploring the interplay between topology, strong electronic correlation, and lattice dynamics[10–14]. Previous studies have demonstrated that a plethora of novel quantum phases, encompassing unconventional superconductivity and spontaneous time-reversal symmetry breaking, can arise in the kagome charge order materials [15–20]. Understanding the genesis and impact of the CDWs within kagome metals constitutes an exciting frontier, imbued with immense potential to provide deep insights into uncharted phases and complex electron-lattice dynamics.

Recently, ScV_6Sn_6 has been recognized as a novel kagome metal with CDW ground state at low temperatures and sparked significant interest[21]. The DFT calculations reveal the existence of two-fold van Hove singularities (VHS) near the Fermi level (E_f) and a Dirac point [Fig. 1(c)], characteristic of kagome metals. However, unlike the prototypical quasi-2D kagome charge order compounds AV_3Sb_5 (A= K, Cs, Rb)[15, 22] and FeGe[9, 23, 24], ScV_6Sn_6 hosts two layers of kagome lattices within a unit cell and exhibits a distinct three-dimensional modulation vector in bulk[21]. Despite being subjected to intensive transport and spectroscopic scrutiny, the nature of the CDW and its interplay with bulk electronic structure and topology remain intensively contested[25–30]. The investigation of bulk electronic structure is greatly obfuscated by the presence of numerous surface states on the multiple terminations, as well as the inherent three-dimension nature of the CDW order. Thus, determining the actual bulk band structure and unearthing the signature of CDW with k_z resolution has become a crucial step towards unraveling the origin and effect of the phase transition, laying the groundwork for its future applications.

In this letter, we successfully disentangle the surface and bulk states of ScV_6Sn_6 by combining high-resolution angle-resolved photoemission spectroscopy (ARPES) and K dosing. We further demonstrate the Z2 topology within the gap of the two-fold VHSs, through revealing the spin-momentum locking of the robust Dirac surface resonance state near the M point. With an enriched understanding of the intricate bulk band structure and DFT calculations, the measured ARPES spectrum across the

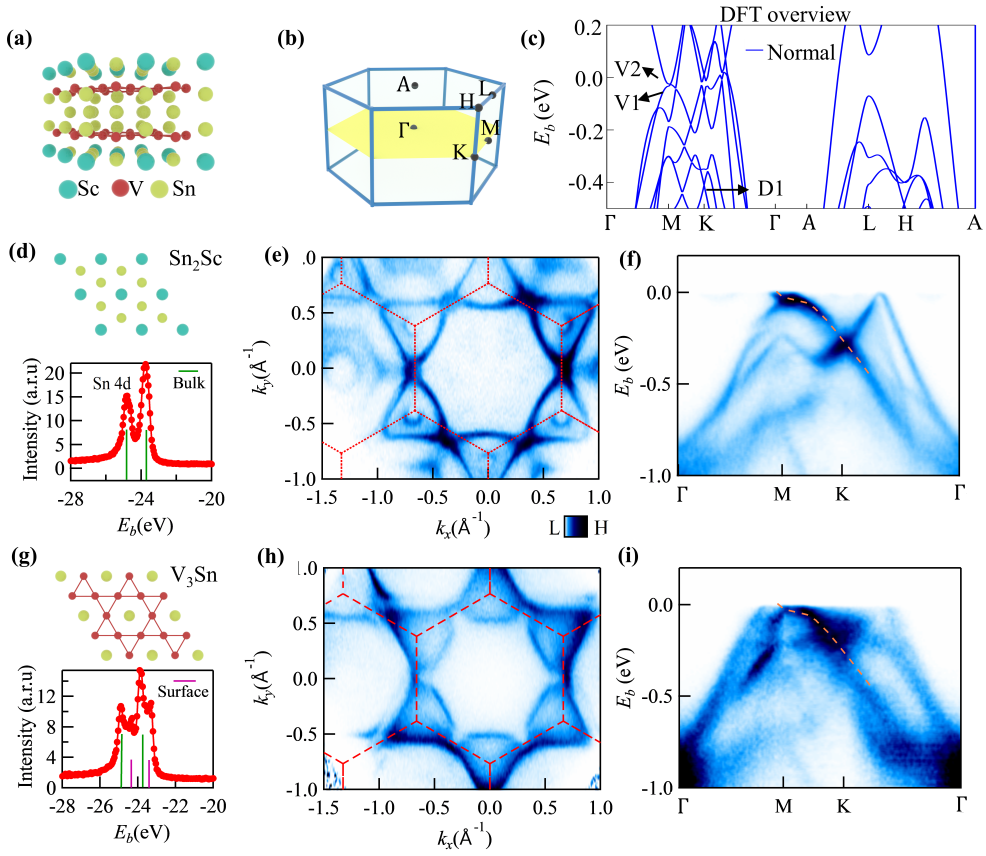

FIG. 1. Termination-dependent band structure in ScV_6Sn_6 . (a) Side view of the crystal structure of ScV_6Sn_6 in the normal phase. (b) Brillouin zone (BZ) and high symmetry points. (c) Theoretical band structure of normal phase of ScV_6Sn_6 . The two types of van Hove singularities (V1 and V2) and Dirac cone (D1) are marked with arrows, respectively. (d) Core-level spectrum of Sn 4d orbitals on the Sc_2Sn layer. The corresponding Fermi surface map, measured with 80 eV photon energy and at 10K, is shown in (e). (f) Energy-momentum cuts along high-symmetry lines. For visual clarity, a dashed line has been plotted at the V2 state. (g), (h) Same with (d-f) but at V_3Sn termination. A notable difference between (e, f) and (h, i) emphasizes the presence of surface states

CDW transition temperature provides unambiguous evidence for $\sqrt{3}\times\sqrt{3}\times3$ charge order and excludes other scenarios.

II. METHODS

High-quality single crystals of ScV_6Sn_6 were grown by the flux method. Starting elements Sc, V, and Sn with a molar ratio of 1: 10: 60 were loaded in an alumina crucible and then sealed in an evacuated silica tube. The tube was then slowly heated to 1373 K, dwelt for 10 hours, and then cooled down to 973 K over 400 hours. Silvery crystals with a hexagonal shape and a typical size of $2\times2\times1$ mm^3 were yielded after centrifugation.

The VUV ARPES measurements were performed at the Electron Spectro-Microscopy (ESM) beamline, National Synchrotron Light Source II, Brookhaven national laboratory. The beam spot was less than 20×10 μm^2. The ScV_6Sn_6 samples were cleaved at 10 K to expose a fresh surface. The energy resolution was better than 20 meV and the angle resolution was 0.2 degree. For the K dosing, we heat the K source with a 5.5 A current for 20 minutes. Several spectra were measured during the process until the energy-momentum cut didn't show further changes. The spin-ARPES measurement was performed at the beamline 10.0.1.2, Advanced Light Source, Lawrence Berkeley National Laboratory. The Soft X-ray ARPES results were obtained at the BL25SU beamline of SPring-8, with an energy resolution of 100 meV. Based on the photon-energy dependence measurement, an inner potential of 16 eV was used for determining the high symmetry energies. Throughout the text, we use the unit cell of the normal phase to determine the BZ. Multiple samples were measured, which yielded consistent results. All the data were measured at the base temperature except the temperature dependence measurement.

We performed *ab initio* calculations in the framework

of density-functional theory within the Perdew-Burke-Ernzerhof exchange-correlation functional [31], as implemented in Vienna ab-initio Simulation Package (VASP) [32]. The all-electron projector augmented-wave method [33] was adopted with $3d^1 4s^2$, $3d^3 4s^2$ and $5s^2 5p^2$ treated as valence electrons for Sc, V and Sn atoms, respectively. A cutoff energy of 400 eV and a dense k-point sampling of the Brillouin zone with a KSPACING parameter of 0.2 were used to ensure the enthalpy converged within 1 meV/atom. We adopted zero damping DFT-D3 van der Waals correction [34] in our calculations. The band topology was calculated from the parity, which was generated by vasp2trace [35]. The post-processing of band and unfolding band calculations was performed by the VASPKIT tool [36]. The surface states calculations were carried out using the combination of Wannier90 [37] and WannierTools [38] software packages.

III. RESULTS AND DISCUSSION

Similar to the other members of a versatile crystal family denoted by the formula ATm_6Sn_6 (A is rare earth or S-block element and Tm is transition metal)[12, 39], ScV_6Sn_6 crystallizes in space group $P6/mmm$, accommodating two A-A stacked V kagome lattices that are sandwiched by the Sn_2Sc layer and Sn layer [Fig. 1(a)]. The weak bonding between V and Sc atoms establishes the natural cleavage plane at the juncture of these two layers[40]. Hence, two terminations, labeled as Sn_2Sc termination and V_3Sn termination, are equally likely to appear in the experiment. In line with our expectations, we observed two distinct Sn-4d core levels (comprising $4d_{\frac{3}{2}}$ and $4d_{\frac{5}{2}}$) during scanning the micro-level beam across the sample surface, as depicted in Fig. 1(d) and Fig. 1(g). The presence of side peaks in Fig. 1(g) implies a distinct chemical environment of Sn atom at the surface comparing to the bulk in this termination. The correspondence between the Sn core levels and terminations is currently under debate[25, 28, 40, 41]. In this paper, we attribute the second type of core level to the polar environment of Sn atom at V_3Sn termination and assign the other one to the Sn_2Sc termination. The assignment finds support in the agreement between the termination-dependent ARPES results, as shown in Figs. 1(e-f, h-i) and surface-projected DFT calculations [Fig. S1[42]]. Notably, the hexagonal Rashba surface state appearing in the second BZ [Fig. 1(e)] is well reproduced in the corresponding surface's calculation [Fig. S1(b)[42]]. Although the bulk Dirac point (D1) and its associated van Hove band may be potentially identified by comparing the energy-momentum cuts along high symmetry lines [Figs. 1(f, i)] of two terminations, the profusion of discrepancies in the spectrum poses a significant challenge in identifying the genuine bulk state and further examining of the effect of bulk charge density wave.

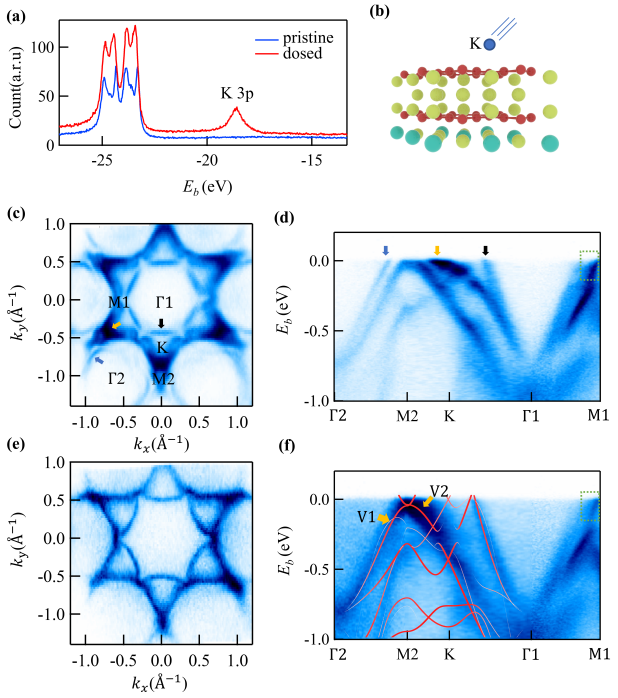

FIG. 2. Unravel the bulk band structure with K dosing. (a) Core level spectrum of Sn 4d state and K 3p state before and after the K dosing. Throughout the dosing process, the number of Sn 4d peaks remains unchanged, confirming measurements taken at the V termination. (b) A schematic provides a visual representation of the K dosing at the V_3Sn termination. (c), (e) The Fermi surface map acquired on the pristine surface (c) and the surface after dosing (e). 129 eV light with linear horizontal polarization was used for collecting the data. (d), (f) Energy-momentum cuts along high symmetry directions, derived respectively from the maps in (c) and (e). The V d-orbital-resolved DFT calculation is overlaid and shows remarkable consistency with the ARPES features near the Fermi level.

To eradicate the surface states induced by the dangling bond of V_3Sn termination, we dosed the V surface with alkaline metal and examined the consequent change in the ARPES spectrum at $k_z = 0$ of the bulk BZ [Figs. 2(a,b)]. Figures 2(c-f) summarize our findings, in which data across multiple BZs and high symmetry lines are incorporated to compensate for the matrix element and sublattice interference effect. Interestingly, after moderate K absorption, the spectrum weight of three states near the E_f [marked with colored arrows in Figs. 2(c-d)] diminishes, indicative of their surface state nature. Notice that the state pointed by the yellow arrow was previously identified as a CDW-driven surface state of the kagome termination[27], and its absence under K dosing indicates the instability of the CDW on the surface. In contrast, bands V1 and V2 exhibit a rigid band shift of approximately -20 meV due to electron doping and form a closed Star-of-David shape pattern at the E_f. As the intensity of a single kagome-driven Dirac band ex-

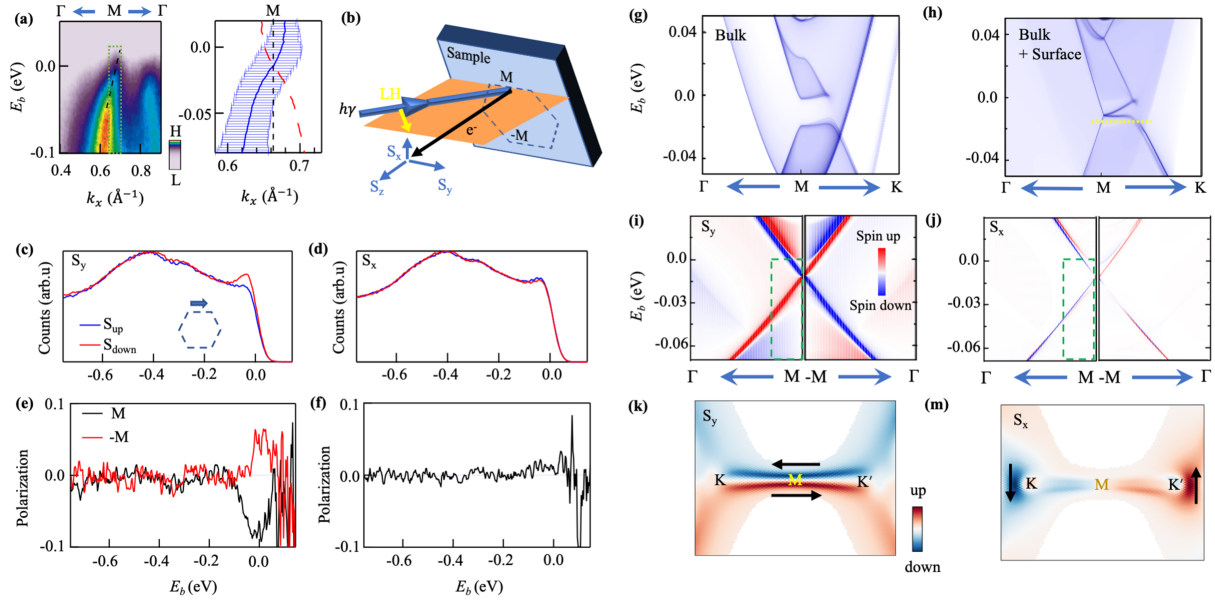

FIG. 3. Spin polarization of the Dirac surface resonance state at the M point. (a) Left: Energy - momentum cut along Γ-M direction, acquired with 50 eV photons. A green rectangle accentuates the detected range of spin EDCs. Right: Extracted and symmetrized dispersion of the S1 state, revealing the full linear crossing around the M point. (b) The geometry of the spin-resolved ARPES measurement. (c), (d) Spin-resolved energy-dispersion curves (EDCs) for the S_y direction (c) and the S_x directions (d). The inset in (c) figures depicts the relative orientation of the spin polarization in relation to the BZ. (e), (f) The binding energy dependence of net spin polarization along S_y and S_x. Data measured at the opposite M point (-M) were plotted and revealed the opposite spin polarization. (g) Surface-projected bulk band structure along Γ - M - K path of the surface BZ. (h) Calculated surface spectrum at V_3Sn termination, in which a singularly-degenerated Dirac state emerges between the two VHSs. (i), (j) Computed spin polarization of the bands near the M point. The green dashed rectangles in (i) and (j) represent the effective detection regions of spin EDCs in (c) and (d), respectively. (k),(m) In-plane spin polarization distribution at binding energy -18 meV (green dashed line in (h)).

hibits BZ-selected behavior due to sublattice interference, such a pattern is consistent with the existence of two distinct van Hove singularities. A thorough analysis of the ARPES spectrum reveals the two van Hove singularities, initially nearly degenerate at E_b = -0.02 eV pre-dosing, shift downwards to E_b = -0.042 eV post-dosing. For the first time of ScV_6Sn_6 , the orbital-decomposed bulk DFT calculation shows remarkable consistency with the post-dosing spectrum along the Γ2-M2-K-Γ1 path, which not only substantiates the assignment of bulk and surface states but also suggests the V1 and V2 VHS originate from $d_{x^2-y^2}$ and d_{z^2} orbitals, respectively (see orbital-resolved calculation in Fig. S2[42]). The quantitative consistency of the band structure also points to the weak electronic correlation of the systems, thereby excluding the possibility of the strong correlation as the driving force of the CDW order[43].

However, a noteworthy state [referred to as S1, circled by the green rectangle in Figs. 2(d,f)] appearing at the M point of the first BZ shows no observable change with K dosing while doesn't align with any bulk state from the DFT calculations. As shown in Fig. 3(a), its linear dispersion closely resembles the Dirac surface state in the topological insulators, and the energy position of the crossing point coincides with the two-fold VHSs. To further investigate the nature of this robust state, we carried out spin-resolved ARPES (SR-ARPES) measurements on the same state at 10 K with 50 eV photons [Figs. 3(a),(b)]. By measuring the spin-resolved energy distribution curve (EDC) around M point [green box in Figs. 3(a),(g).(h)], we observed a clear difference between the spin-up and spin-down EDC curves at E_f for S_y, while negligible difference in S_x [shown in Figs. 3(c-f)]. This result directly demonstrates the direction-selective in-plane spin polarization of the S1 state. Additionally, the polarization flips the sign when measuring at the opposite M point (-M), which indicates the preserved macroscopic time-reversal symmetry within the CDW phase. The consistency of these observations across different photon energies further negates the final state effect (see Fig. S3 in Supplemental Material[42]). The existence of spin polarization serves as direct evidence for the surface state nature of S1, considering the bulk is inversion symmetric.

We computed the surface-projected bulk-band structure and surface states from the first principles, the re-

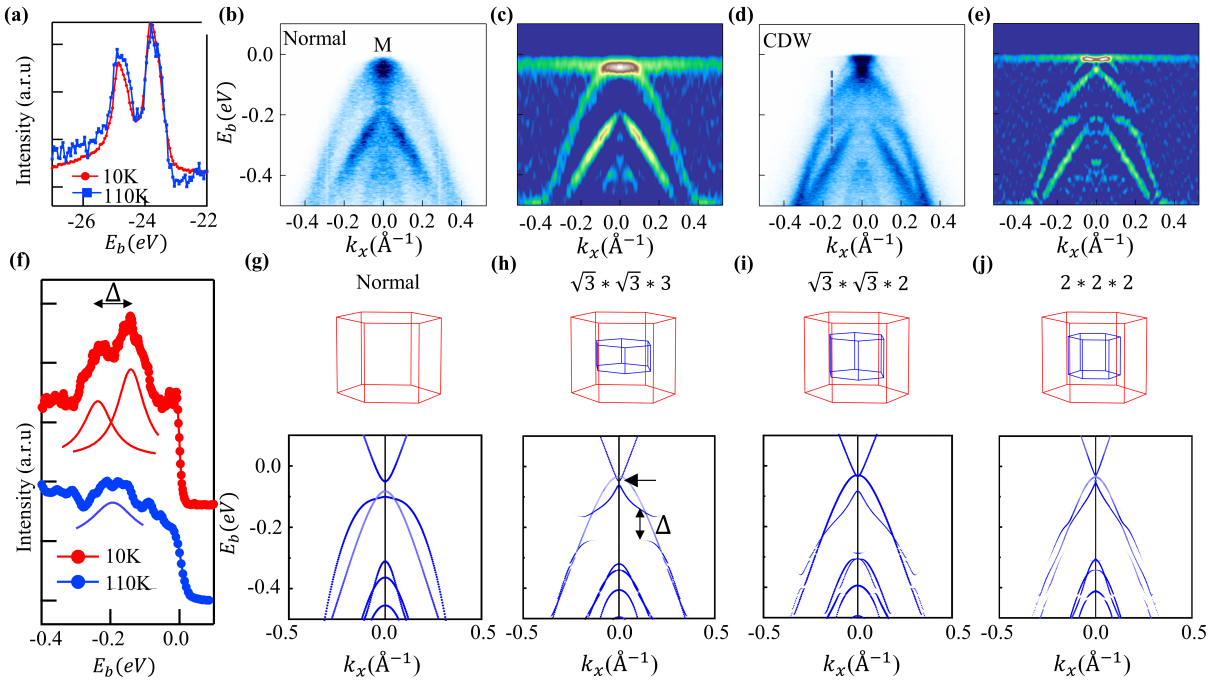

FIG. 4. Direct observation of band folding effect of $\sqrt{3}\times\sqrt{3}\times3$ charge order. (a) Core level spectroscopy of Sn 4d core level measured at both 10 K and 110 K. (b) Cut along Γ - M - Γ direction, obtained with 80 eV photon. Its second derivative is shown in (c). (d), (e) Similar cut with (b-c) but measured below the CDW transition temperature, showing a distinct gap feature below the Fermi level. (f) EDCs cross the gap feature, which are extracted from the dashed line in (d) and the same momentum location in (b). (g), (f) Unfolded band structure in various configurations: the normal phase (g), $\sqrt{3}\times\sqrt{3}\times3$ order (h),$\sqrt{3}\times\sqrt{3}\times2$ order (i) and $2\times2\times2$ charge order (j). The corresponding BZs (red for the normal phase and blue for the CDW phases) are also presented above the calculations. The consistency between (h) and (d) confirms the type of order.

sults of which are shown in Fig. 3(g-h). The calculations confirm the existence of a linear-dispersing surface resonant band between the two VHS bands at the M point on the V_3Sn surface, in agreement with the ARPES observations. Due to the k_z dispersion of the bulk states, the Dirac state overlaps with the bulk-band continuum, and the allowable surface-bulk hybridization may explain its robustness under K dosing. Spin-resolved calculations further demonstrate a pronounced S_y polarization and negligible S_x polarization in the S1 state along Γ – M direction (Fig. 3(i, j)), which fully align with the spin-ARPES observations. We note the vanishing S_x polarization is enforced by the M_y symmetry on the (001) surface. The presence of spin-polarized Dirac surface resonance is a direct consequence of the non-trivial Z2 topology of the V1 band[44] (see details in Fig.S4 of Supplement Material[42]) and therefore is topologically protected. Interestingly, despite the strong anisotropy in the band dispersion, the topological surface resonance exhibits a spin-momentum locking feature (Fig. 3(k-m)), i.e., the spin direction follows the momentum trajectory on a constant energy surface. As the S1 state crosses the Fermi level, its highly anisotropic spin-momentum locking characteristic emerges as a potent mechanism for generating direction-sensitive spin-orbit torque[45], making it a valuable component for future topological spintronics.

Prior research has demonstrated that Scandium and Tin atoms undergo profound out-of-plane displacement in the CDW phase, whereas the Vanadium atom's movement is minimal [21]. Therefore, the bands associated with the Sc and Sn orbitals are anticipated to exhibit greater changes during the phase transition. To directly probe the p orbitals of Sn atoms, we now turn to the Sn_2Sc termination and inspect the CDW's impact on the band structure. We measured the same energy-momentum cut along $\Gamma - M - \Gamma$ at 80 eV, corresponding to $k_z \approx 0.3\pi/c$ (near the BZ boundary of $\sqrt{3}\times\sqrt{3}\times3$ order), below and above CDW transition temperature $T_c =$ 92 K [Fig. 4(a)]. The results and their second derivatives are displayed in Figs. 4(b-e). Above T_c, the main feature near the E_f is a quadratic hole-like band with a band top $E_b =$ -0.03 eV. In the CDW phase, the hole-like band breaks into two distinct bands: namely, a Dirac-like band with crossing energy -0.03 eV and a deeper hole-like band. The breaking point locates at ≈ -0.2 eV and ≈ -0.2 $Å^{-1}$, resulting in a sizable gap Δ of 0.1 eV [Fig. 4(f)]. As the gap is not positioned at E_f and the spectrum

weight diminishes away from the gap, it mainly comes from the intrinsic electronic hybridization between back-folded bands, instead of diffraction of the final states[46]. Meanwhile, no charge order gap at the Fermi level, which lowers the total electronic energy, is observed at this k_z.

The unique band structure transformation at $k_z \approx 0.3\ \pi/c$ imposes strict constraints on the nature of the charge density wave. To elucidate this, we conducted DFT calculations for various possible charge orders within the systems, including 2×2×2 (space group *Immm*), $\sqrt{3}\times\sqrt{3}\times2$ (space group $P6/mmm$) and $\sqrt{3}\times\sqrt{3}\times3$ (space group *R*32) and present the corresponding energy-momentum cut of Sn 4p orbital contribution in Figs. 4(h-j), respectively. We note that a band-unfolding procedure was utilized in the calculation for obtaining the spectrum weight in the first BZ of the normal phase and further facilitating the comparison[47]. Evidently, only the result of the $\sqrt{3}\times\sqrt{3}\times3$ order, which was previously determined via XRD, perfectly matches with the ARPES observation. Other charge orders, despite having lower or comparable ground state energies according to the calculation, fail to account for the valence band gap opening and thus are excluded based on the above argument. Meanwhile, the quadratic band feature can be well captured with the calculation of the normal phase [Fig. 4(f)], further validating the DFT calculations (see more discussion in Figs. (S5,S6) of Supplemental Material[42]).

Interestingly, a recent experiment has observed a collapsed phonon mode with $q = (\frac{1}{3}, \frac{1}{3}, \frac{1}{2})$ below T_c [48]. The absence of a band renormalization that corresponds to $\sqrt{3}\times\sqrt{3}\times2$ order, as demonstrated in this work, hints at the non-static nature of the phonon softening. Concurrently, we observed a large k_z dispersion of the VHS state V2, which is hole-like along $M-L$ with 0.4 eV out-of-plane bandwidth (see Fig. S7(c) in Supplemental Material[42]). In stark contrast to the quasi-2D dispersion of VHSs in CsV_3Sb_5 [49], the out-of-plane dispersion in ScV_6Sn_6 is much larger than the bandwidth of the phonon mode and may impede the nesting conditions of the VHSs and attenuate the divergence of the density of states, despite the fact that the VHSs are near the Fermi level at $k_z = 0$. Those factors are the key to realizing a charge density wave with in-plane Q vector 2×2 [50]. Thus, the comprehensive three-dimensional characteristics of the system must be considered when analyzing the mechanisms underlying the CDW and the absence of superconductivity in ScV_6Sn_6 .

In summary, our study delivers a comprehensive and rigorous examination of the bulk and surface band structure of ScV_6Sn_6 . The identification of the robust topological surface resonance state at M point and the observation of its spin polarization reveals the topology of the system's electronic structure. More importantly, our k_z-resolved ARPES spectrum, substantiated by DFT calculations, directly demonstrates the existence of $\sqrt{3}\times\sqrt{3}\times3$ charge order and the exclusion of other charge orders, offering key insights into the three-dimensional nature of the CDW phase. Our findings lay the foundation for the exploration and manipulation of CDW orders within the growing list of correlated kagome materials.

ACKNOWLEDGEMENTS

The authors thank Haoyu Hu for the fruitful discussions. Work at Princeton University and Princeton-led synchrotron-based ARPES measurements were supported by the U.S. Department of Energy (DOE) under the Basic Energy Sciences program (grant no. DOE/BES DE-FG-02-05ER46200). Theoretical works at Princeton University were supported by the Gordon and Betty Moore Foundation (GBMF9461; M.Z.H.). This research used Beamline 21-ID-1 (ESM-ARPES) of the National Synchrotron Light Source II, a U.S. Department of Energy (DOE) Office of Science User Facility operated for the DOE Office of Science by Brookhaven National Laboratory under Contract No. DE-SC0012704. This research also used resources of the Advanced Light Source, which is a DOE Office of Science User Facility under Contract No. DE-AC02-05CH11231. Synchrotron radiation experiments were performed at the BL25SU of SPring-8 with the approval of the Japan Synchrotron Radiation Research Institute (JASRI) (Proposal No. 2023A1611). Part of this work was financially supported by the Deutsche Forschungsgemeinschaft (DFG) under SFB1143 (project no. 247310070) and the Würzburg-Dresden Cluster of Excellence on Complexity and Topology in Quantum Matter—ct.qmat (EXC 2147, project no. 390858490). Work at Nanyang Technological University was supported by the National Research Foundation, Singapore under its Fellowship Award (NRF-NRFF13-2021-0010) and the Nanyang Assistant Professorship grant. S.R. thanks the Alexander von Humboldt Foundation for a fellowship.

Z.-J. C., S. S., and B. K. contributed equally to this work.

* zijiac@princeton.edu
† guoqing.chang@ntu.edu.sg
‡ mzhasan@princeton.edu

[1] J. A. Wilson, F. Di Salvo, and S. Mahajan, Charge-density waves and superlattices in the metallic layered transition metal dichalcogenides, Adv. Phys **24**, 117 (1975).
[2] G. Grüner, The dynamics of charge-density waves, Rev. Mod. Phys **60**, 1129 (1988).
[3] W. L. McMillan, Theory of discommensurations and the commensurate-incommensurate charge-density-wave phase transition, Phys. Rev. B **14**, 1496 (1976).
[4] J. M. Carpinelli, H. H. Weitering, E. W. Plummer, and

R. Stumpf, Direct observation of a surface charge density wave, Nature **381**, 398 (1996).
[5] J. Chang, E. Blackburn, A. Holmes, N. B. Christensen, J. Larsen, J. Mesot, R. Liang, D. Bonn, W. Hardy, A. Watenphul, et al., Direct observation of competition between superconductivity and charge density wave order in $YBa_2Cu_3o_{6.67}$, Nat. Phys **8**, 871 (2012).
[6] F. Yu, D. Ma, W. Zhuo, S. Liu, X. Wen, B. Lei, J. Ying, and X. Chen, Unusual competition of superconductivity and charge-density-wave state in a compressed topological kagome metal, Nat. Commun **12**, 3645 (2021).
[7] C.-W. Chen, J. Choe, and E. Morosan, Charge density waves in strongly correlated electron systems, Rep. Prog. Phys **79**, 084505 (2016).
[8] B. R. Ortiz, L. C. Gomes, J. R. Morey, M. Winiarski, M. Bordelon, J. S. Mangum, I. W. Oswald, J. A. Rodriguez-Rivera, J. R. Neilson, S. D. Wilson, et al., New kagome prototype materials: discovery of KV_3Sb_5, RbV_3Sb_5, and CsV_3Sb_5, Phys. Rev. Mater **3**, 094407 (2019).
[9] X. Teng, L. Chen, F. Ye, E. Rosenberg, Z. Liu, J.-X. Yin, Y.-X. Jiang, J. S. Oh, M. Z. Hasan, K. J. Neubauer, et al., Discovery of charge density wave in a kagome lattice antiferromagnet, Nature **609**, 490 (2022).
[10] J.-X. Yin, W. Ma, T. A. Cochran, X. Xu, S. S. Zhang, H.-J. Tien, N. Shumiya, G. Cheng, K. Jiang, B. Lian, et al., Quantum-limit Chern topological magnetism in $TbMn_6Sn_6$, Nature **583**, 533 (2020).
[11] L. Ye, M. Kang, J. Liu, F. Von Cube, C. R. Wicker, T. Suzuki, C. Jozwiak, A. Bostwick, E. Rotenberg, D. C. Bell, et al., Massive Dirac fermions in a ferromagnetic kagome metal, Nature **555**, 638 (2018).
[12] Z.-J. Cheng, I. Belopolski, H.-J. Tien, T. A. Cochran, X. P. Yang, W. Ma, J.-X. Yin, D. Chen, J. Zhang, C. Jozwiak, et al., Visualization of tunable Weyl line in A–A stacking kagome magnets, Adv. Mater **35**, 2205927 (2023).
[13] J.-X. Yin, N. Shumiya, S. Mardanya, Q. Wang, S. S. Zhang, H.-J. Tien, D. Multer, Y. Jiang, G. Cheng, N. Yao, et al., Fermion–boson many-body interplay in a frustrated kagome paramagnet, Nat. Commun **11**, 4003 (2020).
[14] S.-Y. Yang, Y. Wang, B. R. Ortiz, D. Liu, J. Gayles, E. Derunova, R. Gonzalez-Hernandez, L. Šmejkal, Y. Chen, S. S. Parkin, et al., Giant, unconventional anomalous Hall effect in the metallic frustrated magnet candidate, KV_3Sb_5, Sci. Adv **6**, eabb6003 (2020).
[15] Y.-X. Jiang, J.-X. Yin, M. M. Denner, N. Shumiya, B. R. Ortiz, G. Xu, Z. Guguchia, J. He, M. S. Hossain, X. Liu, et al., Unconventional chiral charge order in kagome superconductor KV_3Sb_5, Nat. Mater **20**, 1353 (2021).
[16] C. Mielke III, D. Das, J.-X. Yin, H. Liu, R. Gupta, Y.-X. Jiang, M. Medarde, X. Wu, H. C. Lei, J. Chang, et al., Time-reversal symmetry-breaking charge order in a kagome superconductor, Nature **602**, 245 (2022).
[17] T. Neupert, M. M. Denner, J.-X. Yin, R. Thomale, and M. Z. Hasan, Charge order and superconductivity in kagome materials, Nat. Phys **18**, 137 (2022).
[18] B. R. Ortiz, S. M. Teicher, Y. Hu, J. L. Zuo, P. M. Sarte, E. C. Schueller, A. M. Abeykoon, M. J. Krogstad, S. Rosenkranz, R. Osborn, et al., CsV_3Sb_5: A Z2 topological kagome metal with a superconducting ground state, Phys. Rev. Lett **125**, 247002 (2020).
[19] H. Zhao, H. Li, B. R. Ortiz, S. M. Teicher, T. Park, M. Ye, Z. Wang, L. Balents, S. D. Wilson, and I. Zeljkovic, Cascade of correlated electron states in the kagome superconductor CsV_3Sb_5, Nature **599**, 216 (2021).
[20] H. Chen, H. Yang, B. Hu, Z. Zhao, J. Yuan, Y. Xing, G. Qian, Z. Huang, G. Li, Y. Ye, et al., Roton pair density wave in a strong-coupling kagome superconductor, Nature **599**, 222 (2021).
[21] H. W. S. Arachchige, W. R. Meier, M. Marshall, T. Matsuoka, R. Xue, M. A. McGuire, R. P. Hermann, H. Cao, and D. Mandrus, Charge density wave in kagome lattice intermetallic ScV_6Sn_6, Phys. Rev. Lett **129**, 216402 (2022).
[22] Z. Wang, Y.-X. Jiang, J.-X. Yin, Y. Li, G.-Y. Wang, H.-L. Huang, S. Shao, J. Liu, P. Zhu, N. Shumiya, et al., Electronic nature of chiral charge order in the kagome superconductor CsV_3Sb_5, Phys. Rev. B **104**, 075148 (2021).
[23] X. Teng, J. S. Oh, H. Tan, L. Chen, J. Huang, B. Gao, J.-X. Yin, J.-H. Chu, M. Hashimoto, D. Lu, et al., Magnetism and charge density wave order in kagome FeGe, Nat. Phys , 1 (2023).
[24] S. Shao, J.-X. Yin, I. Belopolski, J.-Y. You, T. Hou, H. Chen, Y. Jiang, M. S. Hossain, M. Yahyavi, C.-H. Hsu, et al., Intertwining of magnetism and charge ordering in kagome FeGe, ACS nano (2023).
[25] D. Di Sante, C. Bigi, P. Eck, S. Enzner, A. Consiglio, G. Pokharel, P. Carrara, P. Orgiani, V. Polewczyk, J. Fujii, et al., Flat band separation and robust spin berry curvature in bilayer kagome metals, Nat. Phys , 1 (2023).
[26] H. Tan and B. Yan, Abundant lattice instability in kagome metal ScV_6Sn_6, arXiv preprint arXiv:2302.07922 (2023).
[27] S.-H. Kang, H. Li, W. R. Meier, J. W. Villanova, S. Hus, H. Jeon, H. W. S. Arachchige, Q. Lu, Z. Gai, J. Denlinger, et al., Emergence of a new band and the Lifshitz transition in kagome metal ScV_6Sn_6 with charge density wave, arXiv preprint arXiv:2302.14041 (2023).
[28] S. Lee, C. Won, J. Kim, J. Yoo, S. Park, J. Denlinger, C. Jozwiak, A. Bostwick, E. Rotenberg, R. Comin, et al., Nature of charge density wave in kagome metal ScV_6Sn_6, arXiv preprint arXiv:2304.11820 (2023).
[29] H. Hu, Y. Jiang, D. Călugăru, X. Feng, D. Subires, M. G. Vergniory, C. Felser, S. Blanco-Canosa, and B. A. Bernevig, Kagome materials i: SG 191, ScV_6Sn_6. Flat phonon soft modes and unconventional cdw formation: Microscopic and effective theory, arXiv preprint arXiv:2305.15469 (2023).
[30] Y. Hu, J. Ma, Y. Li, D. J. Gawryluk, T. Hu, J. Teyssier, V. Multian, Z. Yin, Y. Jiang, S. Xu, et al., Phonon promoted charge density wave in topological kagome metal ScV_6Sn_6, arXiv preprint arXiv:2304.06431 (2023).
[31] J. P. Perdew, K. Burke, and M. Ernzerhof, Generalized gradient approximation made simple, Phys. Rev. Lett **77**, 3865 (1996).
[32] G. Kresse and J. Furthmüller, Efficient iterative schemes for ab initio total-energy calculations using a plane-wave basis set, Phys. Rev. B **54**, 11169 (1996).
[33] P. E. Blöchl, Projector augmented-wave method, Phys. Rev. B **50**, 17953 (1994).
[34] S. Grimme, J. Antony, S. Ehrlich, and H. Krieg, A consistent and accurate ab initio parametrization of density functional dispersion correction (DFT-D) for the 94 elements H-Pu, The Journal of chemical physics **132** (2010).

[35] M. Vergniory, L. Elcoro, C. Felser, N. Regnault, B. A. Bernevig, and Z. Wang, A complete catalogue of high-quality topological materials, Nature **566**, 480 (2019).

[36] V. Wang, N. Xu, J.-C. Liu, G. Tang, and W.-T. Geng, VASPKIT: A user-friendly interface facilitating high-throughput computing and analysis using VASP code, Comput. Phys. Commun **267**, 108033 (2021).

[37] G. Pizzi, V. Vitale, R. Arita, S. Blügel, F. Freimuth, G. Géranton, M. Gibertini, D. Gresch, C. Johnson, T. Koretsune, J. Ibañez-Azpiroz, H. Lee, J.-M. Lihm, D. Marchand, A. Marrazzo, Y. Mokrousov, J. I. Mustafa, Y. Nohara, Y. Nomura, L. Paulatto, S. Poncé, T. Ponweiser, J. Qiao, F. Thöle, S. S. Tsirkin, M. Wierzbowska, N. Marzari, D. Vanderbilt, I. Souza, A. A. Mostofi, and J. R. Yates, Wannier90 as a community code: new features and applications, Journal of Physics: Condensed Matter **32**, 165902 (2020).

[38] WannierTools : An open-source software package for novel topological materials, Computer Physics Communications **224**, 405 (2018).

[39] W. Ma, X. Xu, J.-X. Yin, H. Yang, H. Zhou, Z.-J. Cheng, Y. Huang, Z. Qu, F. Wang, M. Z. Hasan, et al., Rare earth engineering in RMn_6Sn_6 (R= Gd- Tm, Lu) topological kagome magnets, Phys. Rev. Lett **126**, 246602 (2021).

[40] Y. Hu, X. Wu, Y. Yang, S. Gao, N. C. Plumb, A. P. Schnyder, W. Xie, J. Ma, and M. Shi, Tunable topological Dirac surface states and van Hove singularities in kagome metal GdV_6Sn_6, Sci. Adv **8**, eadd2024 (2022).

[41] S. Peng, Y. Han, G. Pokharel, J. Shen, Z. Li, M. Hashimoto, D. Lu, B. R. Ortiz, Y. Luo, H. Li, et al., Realizing kagome band structure in two-dimensional kagome surface states of RV_6Sn_6 (R= Gd, Ho), Phys. Rev. Lett **127**, 266401 (2021).

[42] See Supplemental Material at [link] for Soft-Xray ARPES results; Further discussion on the spin-resolved ARPES and spin-EDCs at 80 eV; Surface state calculation of different terminations; Orbital-decomposed band structure calculations; Total energies and electronic band structure calculations for various CDW configurations., .

[43] J. A. Sobota, Y. He, and Z.-X. Shen, Angle-resolved photoemission studies of quantum materials, Rev. Mod. Phys **93**, 025006 (2021).

[44] L. Fu and C. L. Kane, Topological insulators with inversion symmetry, Phys. Rev. B **76**, 045302 (2007).

[45] Q. Shao, P. Li, L. Liu, H. Yang, S. Fukami, A. Razavi, H. Wu, K. Wang, F. Freimuth, Y. Mokrousov, et al., Roadmap of spin–orbit torques, IEEE Transactions on Magnetics **57**, 1 (2021).

[46] M. D. Watson, A. Louat, C. Cacho, S. Choi, Y. H. Lee, M. Neumann, and G. Kim, Spectral signatures of a unique charge density wave in Ta_2NiSe_7, Nat. Commun **14**, 3388 (2023).

[47] P. V. Medeiros, S. Stafström, and J. Björk, Effects of extrinsic and intrinsic perturbations on the electronic structure of graphene: Retaining an effective primitive cell band structure by band unfolding, Physical Review B **89**, 041407 (2014).

[48] A. Korshunov, H. Hu, D. Subires, Y. Jiang, D. Călugăru, X. Feng, A. Rajapitamahuni, C. Yi, S. Roychowdhury, M. Vergniory, et al., Softening of a flat phonon mode in the kagome ScV_6Sn_6, arXiv preprint arXiv:2304.09173 (2023).

[49] M. Kang, S. Fang, J.-K. Kim, B. R. Ortiz, S. H. Ryu, J. Kim, J. Yoo, G. Sangiovanni, D. Di Sante, B.-G. Park, et al., Twofold van Hove singularity and origin of charge order in topological kagome superconductor CsV_3Sb_5, Nat. Phys **18**, 301 (2022).

[50] T. Rice and G. Scott, New mechanism for a charge-density-wave instability, Phys. Rev. Lett **35**, 120 (1975).